CHIMIA 48 (1994) Nr. 3 (März)

Chimia 48 (1994) 64–71

ISSN 0009–4293

Advances in Surface Analysis and Mass Spectrometry Using Laser Desorption Methods

Renato Zenobi*

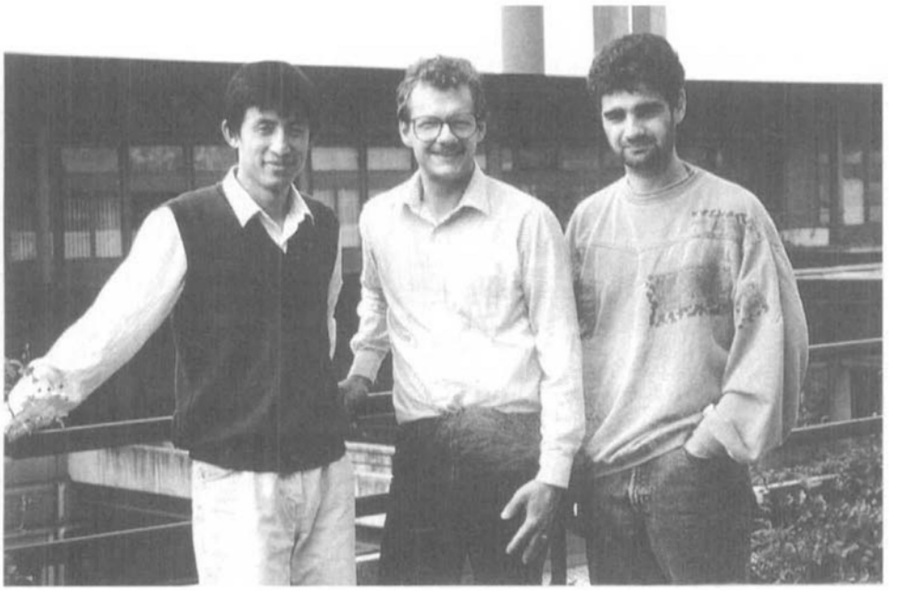

From left to right: *Qiao Zhan*, *Renato Zenobi*, *Pierre Voumard*

Renato Zenobi, born in 1961 in Zürich, went through school and college there and graduated from ETH-Zürich in 1986. His diploma thesis, done under the direction of Prof. *Martin Quack* was on IR overtone spectroscopy and photoacoustical spectroscopy of the C–H oscillator in CD_3COH. He then started graduate school at Stanford University (USA) with Prof. *Richard N. Zare*. He finished his Ph. D. thesis on two-step laser mass spectrometry in 1990 and subsequently continued his scientific education with two postdoctoral appointments, first at the Surface Science Center of the University of Pittsburgh (with Prof. *John T. Yates*) and later at the University of Michigan (with Prof. *Raoul Kopelman*). In 1991, he won the first *Alfred Werner* Fellowship which allowed him to return to Switzerland and to start building up his own research laboratory. His group, hosted since 1992 by the Ecole Polytechnique Fédérale in Lausanne, is active at the interface of physical and analytical chemistry, investigating laser-surface interactions, laser desorption mechanisms, matrix-assisted laser desorption/ionization (MALDI), and the application of laser mass spectrometry to biochemical and environmental problems.

Renato Zenobi has won several awards and fellowships, among which are the *Thomas Hirschfeld* award (1989), and *Andrew Mellon* Postdoctoral Fellowship (1990), and most recently the *Ruzicka* Prize (1993).

Abstract. Laser desorption methods have profoundly influenced surface analysis and mass spectrometry. They provide snapshots of surface processes and allow detection of minute quantities of surface adsorbates. They allow the intact vaporization of polar, nonvolatile, high molecular weight, and thermally labile compounds that would otherwise be inaccessible to gas-phase studies. This contribution presents some recent advances in the field of laser desorption from surfaces, describes the experimental realization of a two-step laser mass spectrometer, highlights new insights into the mechanism of laser-induced thermal desorption, and illustrates the practical usefulness of the methodology with selected analytical examples.

1. Introduction

Lasers are being used increasingly in surface science and for mass-spectrometric studies. They are of interest for these fields because of their high power density, short pulse widths, high spectral purity, and spatial coherence, allowing them to be focused onto very small spots on a surface. They are also being used for machining and patterning [1–4] of material surfaces, polymer surfaces and even biological tissue. However, lasers have made their greatest scientific impact in surface science as a powerful new way of studying adsorbate layers. This is being done *in situ* with modern nonlinear spectroscopic methods such as second harmonic generation (SHG), sum-frequency generation (SFG) [5], or surface-enhanced *Raman* spectroscopy (SERS) [6], with ultrafast laser pulses to probe dynamical surface processes [7][8], and with desorption methods to gain access to complex surface adsorbates in the gas phase [9–11]. Laser methods have also been used successfully to detect intermediates of surface reactions [12–14], which is important for the understanding of catalytic reaction pathways.

Perhaps the most successful application of lasers in the context of surface analysis is to employ them for desorption of adsorbed molecules, followed by high-resolution and sensitive gas phase spectroscopic methods for detection, *e.g.* mass spectrometry. The potential of using laser desorption methods for gaining access to complex nonvolatile molecules in the gas phase has already been realized in the late seventies. This original form of Laser Desorption Mass Spectrometry (LDMS) was performed in a fashion analogous to other methods for direct ion production from nonvolatile solids, such as Secondary Ion Mass Spectrometry (SIMS), Fast Atom Bombardment (FAB), or Plasma Desorption Mass Spectrometry (PDMS). LDMS utilizes one single laser source (pulsed or cw) to perform desorption and ionization in a single step. A laser beam is focused directly on the solid sample deposited on a direct inlet probe. LDMS is primarily used for the analysis of inorgan-

**Correspondence*: Dr. Renato Zenobi
LPAS (chimie)
Ecole Polytechnique Fédérale
CH-1015 Lausanne

ic nonvolatile materials and elemental analysis of surfaces, but as early as 1978, LDMS was applied to fairly complex organic and bio-organic molecules. *Kistemaker* and coworkers published impressive LDMS data of thermally labile substances such as sucrose (*m/z* 342) and digitonin (*m/z* 1228), setting a high mass record at this time with the latter substance [15]. The success of the LDMS technique also led to a commercial instrument based on a time-of-flight mass spectrometer (LAMMA, *Leybold Haereus*), mainly celebrated as a laser microprobe instrument for surface studies with *ca.* 2 μm spatial resolution. The basic drawbacks of direct laser desorption/ionization are a strong matrix effect on ionization, and the inability for the operator to control the sample volatilization and ionization process independently.

In 1988, Matrix-Assisted Laser Desorption/Ionization (MALDI) was introduced by *Karas* and *Hillenkamp* as a method for the production of parent ions from large and very large nonvolatile molecules [16]. This method was originally developed from LDMS with the idea to add to the analyte a chemical matrix that strongly absorbs the wavelength of the desorption laser. The matrix was supposed to promote efficient desorption of the fragile analyte molecules. But it was soon found that this sample preparation method had two other, highly beneficial effects. A high excess of matrix (100 : 1–100000 : 1) chemically isolates the analyte molecules, and upon pulsed laser desorption, they are 'cooled' by the rapidly expanding plume of matrix much like in a seeded supersonic jet [17][18]. The matrix also mediates the ionization of the analyte in the dense desorption plume. The processes responsible for the production of intact parent ions are still not understood in detail, and good matrices, *e.g.* sinapinic acid, nicotinic acid, or 2,5-dihydroxybenzoic acid, are usually found by intuition or by trial and error methods. However, it is the chemical properties of the matrix that may ultimately give the experimentalist control over the ion formation step in MALDI, a degree of freedom that is essentially missing in the LDMS technique. MALDI has rapidly become a highly successful method, in particular for the mass spectrometric analysis of synthetic polymers [19][20] and biopolymers such as proteins and oligonucleotides [17][21] up to molecular weights of several 100,000 amu.

Ultimate control over the two processes, desorption and ionization, can be attained, if they are separated in space and in time, and if they can be optimized individually. Many combinations between pulsed desorption methods with postionization techniques are possible and are being practised [22–27], but we prefer an embodiment where desorption is accomplished with a far IR laser pulse, followed by ionization with a pulsed UV laser. This approach is dubbed two-step laser mass spectrometry [10][28] and its experimental realization is presented in the next section.

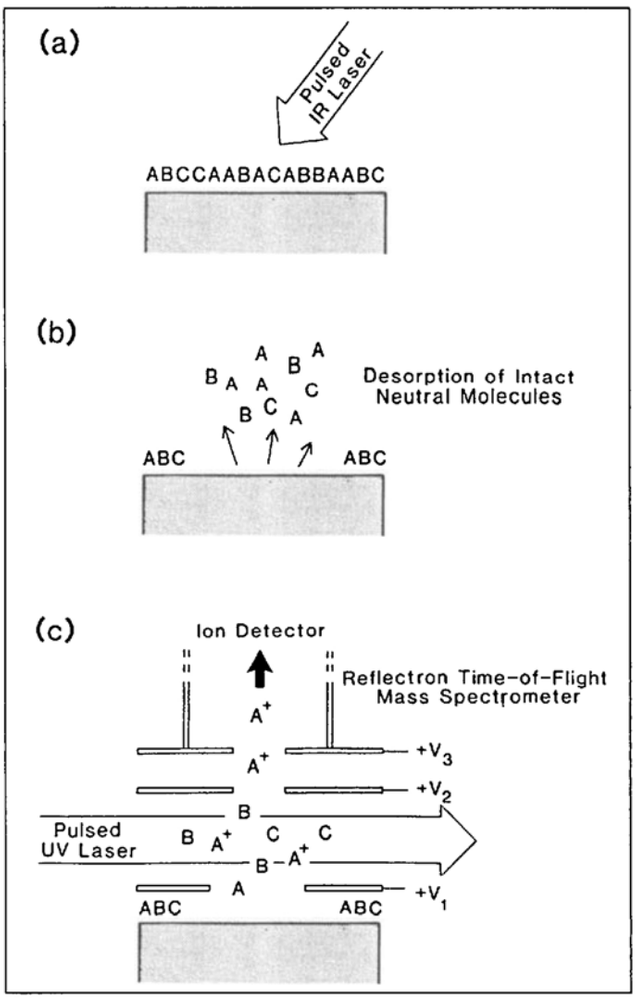

Fig 1. a) *Laser-induced rapid heating of a sample by a CO_2 laser pulse;* b) *thermal desorption of intact neutral molecules from the surface;* c) *resonance-enhanced multiphoton ionization of desorbing molecules by an UV laser pulse serves as an efficient, optically selective, and soft ionization process.* The ions produced are extracted by an electric field and mass-separated in a reflectronTOF mass spectrometer.

2. Two-Step Laser Mass Spectrometry: Experimental Realization and Performance

Several instruments for two-step laser mass spectrometry (L2MS) have been constructed by various groups [28–31], some with the capability for microprobing of the sample surface [32–34]. As an example, an L2MS setup built in our laboratory at EPFL, Lausanne, is discussed in this section.

Fig. 1 schematically shows the succession of events in two-step laser mass spectrometry. A line-tuneable pulsed CO_2 laser (*Lumonics* model TE-821HP) that can deliver up to 1 J in 100 ns heats the sample surface extremely rapidly and desorbs intact analyte molecules (*Fig. 1a*). The rapid laser-induced thermal desorption process causes intact neutral molecules to be released from the substrate surface (*Fig. 1b*).

The crucial step for optically selective and efficient soft ionization is the resonance-enhanced multiphoton ionization (REMPI) method used for the second step (*Fig. 1c*). The REMPI mechanism for the case of two-photon ionization works as follows: a first photon induces a transition to an excited state only for those molecules that absorb the laser wavelength. Then, a second photon ionizes the excited molecules. Since different molecules have different UV absorption spectra, one can preferentially ionize certain classes of molecules by choosing the wavelength to coincide with a maximum in their UV spectrum. Ionization by REMPI is orders of magnitude more efficient than nonresonant multiphoton ionization of molecules that lack a suitable chromophore [35]. For making use of this optical selectivity, it is,

therefore, of great importance to have a tunable UV source. We use a frequency doubled dye laser (*Lambda Physik* FL 2002) pumped by an excimer laser (*Lambda Physik* FMG 201 MSC at 308 nm) with *ca.* 20-ns pulse width. This ionization method has several advantages: a power density of *ca.* 10^6 W/cm^2 provides a high fraction of ionized molecules and, therefore, high sensitivity, and since the ionization takes place in the gas phase, it is free of matrix effects. Furthermore, it is a 'soft' ionization method: no or very little fragmentation occurs, and parent ions dominate the mass spectra. This greatly reduces the complexity of mass spectra from complicated mixtures. However, as demonstrated in *Sect. 4*, fragmentation can also be chosen to occur by increasing the laser power density. This can be useful for structure elucidation.

In our instrument, a cylindrical lens focuses the UV beam to a ribbon that lies on an equipotential plane between the first two electrodes (*Fig. 1c*). To maximize the sensitivity of the apparatus, the UV laser beam passes only 2 mm above the sample surface in order to ionize a large number of desorbing neutrals. A delay generator triggers the lasers so that the UV laser is fired at the maximum of the temporal distribution of the plume of the desorbed neutrals.

The three electrodes that establish the extracting and accelerating fields form a conventional *Wiley-MacLaren* [36] extraction region for time-of-flight (TOF) mass spectrometry. TOF Mass spectrometers are the natural choice for ions produced instantaneously, *e.g.*, by pulsed lasers, and they are celebrated for their simplicity and high ion transmission, which results in high sensitivity of the instrument. Mass analysis is performed in a reflectron TOF mass spectrometer (*R.M. Jordan Co.*), and ions are detected by a pair of microchannel plates. The whole vacuum system is pumped by two turbo molecular pumps to 10^{-6} mbar in the ionization region and to 10^{-7} mbar in the TOF tube/detector chamber.

2.1. *Spatial Resolution*

The spatial resolution for desorption is ultimately limited by the diffraction limit. The *Rayleigh* resolution condition for a *Gaussian* beam with wavelength λ, focused through a lens under an aperture angle α in a medium with refractive index n is given in [37]:

$$d_{min} = \frac{0.61\,\lambda}{n \sin \alpha} \qquad (1)$$

It is, therefore, very important to bring the focusing lens close to the surface under investigation for achieving a good spatial resolution. In our instrument, the desorption laser beam enters the vacuum chamber under a 45° angle through a short focal length (5 cm) ZnSe spherical lens that is mounted on the inside end of a long metal tube protruding into the chamber. For adjusting the focus, the whole tube that holds the focusing lens can be moved in and out by a linear translator with micrometer resolution. To visualize the desorption spot through another window in the vacuum chamber, a He-Ne laser propagates collinearly with the CO_2 laser. We measured desorption spot sizes by focusing the CO_2 laser on thick dye layers by measuring under an optical microscope the holes created in such films by several tens to hundreds of laser shots. The minimum spot size we were able to obtain was 20 μm, very close to the calculated diffraction limit. A spatial resolution in the micrometer range opens possibilities for interesting analytical studies with spatial resolution, *e.g.* comparing the composition of individual μ-size particles.

2.2. *Sensitivity*

To obtain quantitative information on the sensitivity of our instrument, a homogeneous sample film on a solid substrate was necessary. A series of coronene solutions were prepared with concentrations C (C = 2.6 x 10^{-11} mol/ml), $C/10$, and $C/100$. One drop (2–3 ml) of the solution was deposited on the surface of glass microscope slide which was spun at *ca.* 1000 RPM. To recognize the area covered by the solution, *Du Pont* oil red was added to the solution (the dye/coronene ratio was 10^3–10^5). The coronene surface concentration was calculated from the concentration of the solution and the area covered by the drop. Using an ionization wavelength of 308 nm, mass spectra of a layer containing 7 x 10^{-11} mol/cm^2 coronene were obtained, which corresponds to only 32 fmol of the substance within the laser spot. The coronene signal was observed for each single shot, and the signal persisted for *ca.* 150 shots. From this, we calculate a detection limit (signal/noise = 3) of ≈20 attomoles/laser shot, which corresponds to a surface coverage of 10^{-4} monolayers of coronene. The coronene signal was also found to be linear with surface concentration over at least three orders of magnitude. We note that L2MS is probably the most sensitive method available today for the detection of *molecular* surface adlayers.

2.3. *Mass Resolution*

The mass resolution in a TOF mass spectrometer is given as $M/\Delta M = t/2\Delta t$, where t is the flight time of an ion package and Δt its FWHM. While linear TOF mass spectrometers have rather poor resolution, the use of a reflectron improves the mass resolution by one or two orders of magnitude [38]. The spectra shown in the figures in *Sect. 4* reach a maximum mass resolution of *ca.* 1000. However, this resolution is limited by the ionization laser pulse width (Δt = 20–25 ns). We can increase the mass resolution by reducing the extraction potential of the ion source, which leads to a longer flight time t. Using coronene as a test substance, $M/\Delta M$ was determined to be *ca.* 2000 for these tests. Under these conditions, Δt was still measured to be *ca.* 25 ns. Therefore, the ultimate resolution of our instrument is not determined, but certainly exceeds 2000. However, by reducing the extraction and reflection potentials, the sensitivity of the instrument is slightly reduced. If a very high mass resolution is not needed, the potential settings are optimized for highest sensitivity.

3. Mechanism of Laser-Induced Thermal Desorption

It is presently not fully understood why labile molecules can be desorbed by pulsed laser radiation without fragmentation. To gain more insight into the laser desorption mechanism, we have started a research project with aniline ($PhNH_2$) adsorbed on quartz (SiO_2) as a model system, using a well-controlled environment (ultrahigh vacuum, submonolayer films). Quartz is a technologically important material that also serves as a substrate for practical applications in laser desorption mass spectrometry. Aniline can interact with surfaces in a number of different ways, and it is large enough to resemble the behavior of high molecular weight compounds in desorption experiments. On the other hand, $PhNH_2$ is small enough to be introduced into the ultrahigh vacuum system as a vapor, its spectroscopy is well understood [39–42], and its interaction with quartz can be studied in detail ([43][44] and ref. cit. therein). From such studies, a desorption activation energy of $E_a \approx 140$ kJ/mol, and a desorption preexponential factor of $\nu \approx 10^{17}$ s^{-1} have been found for submonolayer films.

Several mechanisms have been suggested to explain the non-destructive nature of pulsed laser-induced thermal desorption: *i*) for 'real world samples', it is possible that enough small molecules are

present to promote the desorption of non-volatile large compounds in a 'steam-assisted' or jet-like desorption process, similar to matrix-assisted laser desorption [16–18]. This mechanism can be distinguished from others by translational and internal state distributions similar to those of a seeded molecular beam expansion [18][45]. *ii*) It has often been argued that laser desorption must be some kind of nonequilibrium process, where the available energy breaks the surface-adsorbate bond rapidly, but does not randomize in the whole surface-adsorbate system on the time scale of the desorption event [46]. The validity of such a mechanism depends both on the heating rate and the strength of the surface-adsorbate bond. If valid, internally cold or 'lukewarm' desorbing molecules will be found in the desorption plume. *iii*) The predominance of desorption over decomposition may also be the result of thermal equilibrium kinetics at high temperatures. In the high-temperature regime, where pre-exponential factors dominate the kinetics, desorption has been found to be favored over decomposition for a number of adsorbates [47]. The clue for intact desorption in this mechanism is to reach the high-temperature regime rapidly, before significant decomposition occurs.

If a thermal equilibrium mechanism is indeed valid, the desorption can be described by an *Arrhenius*-type equation, which, in the context of surface processes is often called *Polanyi-Wigner* equation or *Frenkel* equation:

$$-\frac{d\theta}{dt} = \theta^n \cdot \nu \cdot \exp\left(\frac{-E_a}{kT}\right) \qquad (2)$$

Here θ is the fractional surface coverage, n is the desorption order, ν is the pre-exponential factor, E_a is the desorption activation energy, t is the time, and T the temperature. *Eqn. 2* describes the rate of the surface process considered (in our case, desorption) measured as a decrease of the surface coverage per unit time. It is interesting to study *Eqn. 2* for different heating rates, defined as $\beta = dT/dt$. For this purpose we re-write equation *Eqn. 2*, assuming a first-order process ($n = 1$) as

$$-\frac{d\theta}{\theta} = \frac{\nu}{\beta} \cdot \exp\left(\frac{-E_a}{kT}\right) dT \qquad (3)$$

The left-hand side can easily be integrated analytically, whereas the right-hand side is solved by numerical methods. As a result, we obtain the surface coverage as a function of temperature, dependent also on the parameters β, ν, and E_a. The steepest decrease of $\theta(T)$ occurs at the temperature T_{des} where the maximum in a classical temperature-programmed desorption (TPD) experiment lies. Such TPD curves can be simulated by calculating numerically $-d\theta/dT$ from *Eqn. 3*. If β is increased, the TPD maximum T_{des} shifts to higher temperatures. This has been known for a long time [48], as β needs to be sufficiently well determined to extract meaningful information from a TPD curve. It is also clear intuitively: as an adsorbate-covered surface is heated more rapidly, the system is more easily 'superheated', before desorption of the adlayer is complete. With laser heating, however, this superheating can be taken to an extreme, since heating

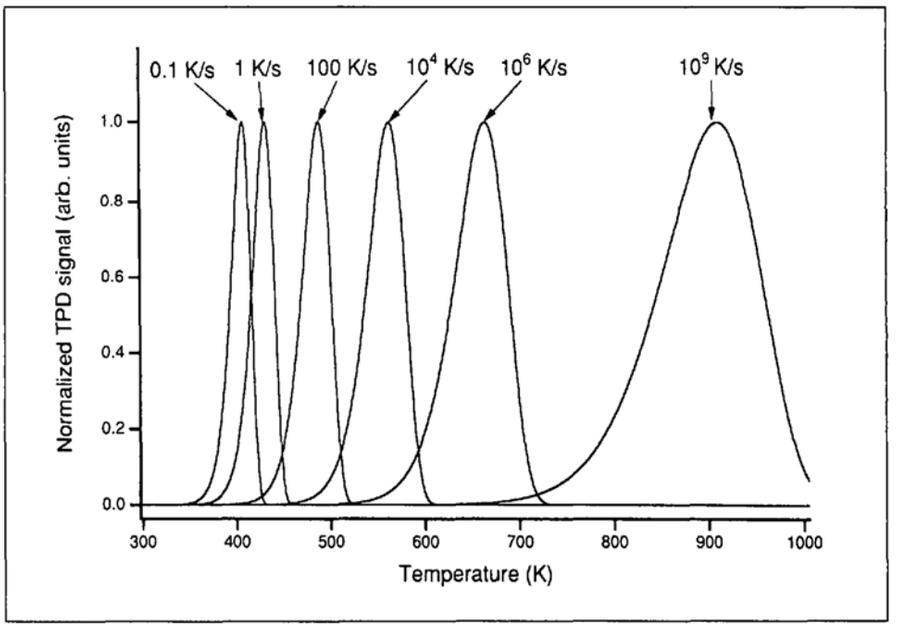

Fig 2. *Simulated temperature-programmed desorption (TPD) curves, calculated by numerical integration of* Eqn. 3, *for various linear heating rates* β. Desorption parameters are taken from measurements on the system $PhNH_2$/quartz ($\nu = 10^{17}$ s^{-1}; $E_a = 140$ kJ/mol). A simple trapeze method was adapted for numerical integration, with 1K temperature steps. This leads to an overestimation of the desorption temperature T_{des} by *ca.* 10%.

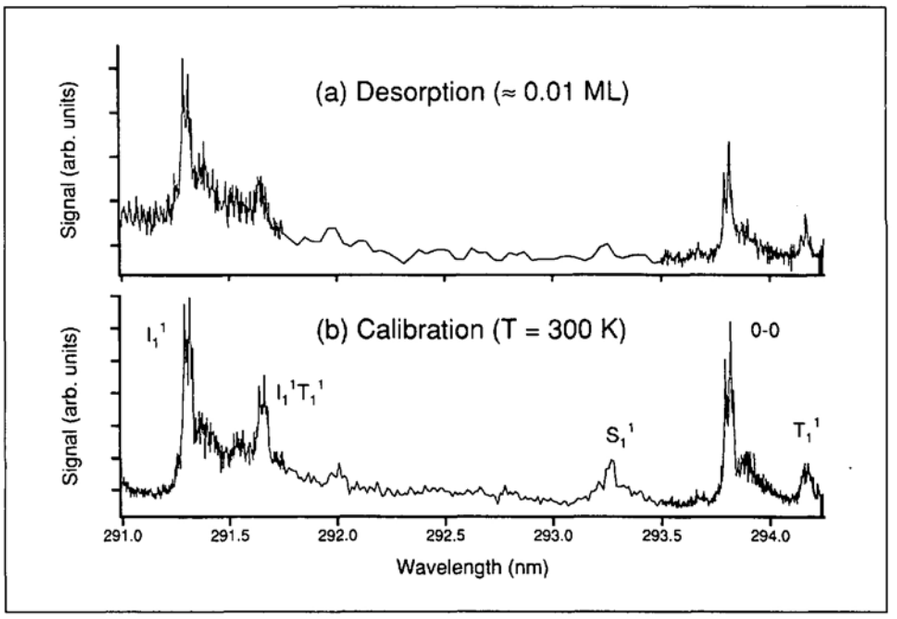

Fig. 3. *REMPI Spectrum of $PhNH_2$ a) laser-desorbed from a submonolayer surface coverage on quartz and* b) *in a calibration measurement taken at 300 K and 5 x10^{-6} mbar pressure.* The identification of various hot bands visible in the spectrum is given in [39–42]. The unambiguously assigned I_1^1 band is used to calculate the vibrational temperature of the aniline. The vibrational temperature of laser-desorbed aniline is found to be close to 300 K.

rates up to 10^{10} K/s are attained [49][50]. *Fig. 2* illustrates this behavior, calculated for our model system $PhNH_2$/ quartz: At high heating rates, the system is superheated to *ca.* 900 K, *i.e.*, desorption occurs at a temperature far higher than if classical heating rates are employed. In addition, the width of the desorption feature increases to over 100 K.

These results should be compared with measurements of the energy in various degrees of freedom of laser-desorbed aniline molecules. For example, recording of the REMPI spectrum provides access to a vibrational temperature, by comparing the population in the vibrational ground state with that in vibrationally excited states. This information can be obtained from relative intensities of vibrational hot bands seen in the REMPI spectrum (see *Fig. 3*). A particularly interesting transition, labeled I_1^1) in the spectrum, originates from one quantum of vibrational excitation of the $-NH_2$ inversion mode, located only 40 cm^{-1} above the vibrational ground state. (The position of the hot bands in the REMPI spectrum may be found either to the blue or to the red of the 0-0 transition, depending both on the ground-state and electronically excited-state vibrational structure of the transition considered.) Our data indicates a vibrational temperature close to 300 K for $PhNH_2$ laser-desorbed from a submonolayer coverage on quartz. In fact, quite a substantial difference seems to exist between the vibrational temperature ($T_{vib} \approx 300$ K) and the calculated desorption temperature ($T_{des} \approx 900$ K) for laser desorption conditions. This may indicate that a thermal equilibrium does not exist, which is somewhat surprising, since the desorption process is still fairly slow (ns timescale) compared to intramolecular vibrational redistribution processes (ps timescale). We are currently studying the reasons for this effect.

4. Applications of Two-Step Laser Mass Spectrometry

4.1. *Mass Spectrometric Analysis of Complex Molecules*

Fig. 4 shows one example of a series of mass spectrometric studies conducted with L2MS on synthetic porphyrin dimers and trimers [51]. Compounds such as the one shown in *Fig. 4* are of interest, because they have been hypothesized to have tumor-localizing properties [52–55], and they could be used for laser cancer detection and phototherapy [56]. Our goal in this investigation was *i*) the mass-spectrometric detection of these non-volatile and thermally labile compounds, and *ii*) their structural elucidation. For this reason, an ionization laser power density of *ca.* 1.5 x 10^5 W/cm^2 was used to induce some fragmentation. That fragmentation occurs is clearly seen from the distribution of signals in the dimer (*ca.* 1100–1200 amu) and monomer (*ca.* 550–610 amu) regions in the spectrum. Furthermore, a metastable signal is found at *ca.* 730 amu. If the laser power density is reduced by *ca.* a factor of 10, the fragmentation disappears almost completely, and the parent ion of the dimer dominates the L2MS spectrum [51].

Other signals are seen in this L2MS spectrum, most notably mass standards in the low mass range (marked with *). The signal at 652 cannot be explained as a fragment originating from the analyte molecule, and is interpreted as contamination or by-product from the synthesis, respectively. There are also several signals at masses higher than the parent ion peak at 1198 amu. These are probably due to adducts, *e.g.* $(M+Na)^+$ at 1221 amu.

All of the fragment peaks can be interpreted using the structure shown in *Fig. 4* and known fragmentation mechanisms, and they can, therefore, be used for structural elucidation. Examples include the cleavage of the ether linkage between the two porphyrin rings, leading to *m/z* 591 and 608, fragmentation of porphyrin ring substituents (1183, $M - CH_3$; 1172, $M - C_2H_2$; 1139, $M - COOCH_3$ *etc.*). Some fragmentations involve a rearrangement process, *e.g.*, the formation of 1172 ($M - CO_2$), favored by the stability of the CO_2 molecule as a leaving group. Similar, but less intense fragmentation is also observed to occur starting from monomer peaks (*e.g.*, 565 = 591 – C_2H_2; 579 = 608 – CHO). Our data also documents the applicability of L2MS to high mass compounds. Several porphyrin dimers as well as a porphyrin trimer (*m/z* 1670) were studied.

4.2. *Mixture Analysis*

The fact that parent ions can also be produced with virtually no fragmentation, using *soft ionization conditions* with lower laser power densities, makes L2MS a good candidate for the chemical analysis of sample mixtures. Furthermore, the resonance-enhanced laser ionization method used provides a degree of optical selectivity that renders complicated sample preparation procedures unnecessary. In many cases, complex sample mixtures can directly be introduced into the desorption region of the instrument, and the choice of ionization laser conditions (wavelength, pulse width, power density) defines the classes of molecular chromophores that will be detected efficiently.

In this section, L2MS spectra from rather complex mixtures are presented. The first example is a sample of petroleum pitch characterized by a high melting point and little soluble aromatic carbon contents. This material is used for impregnation purposes and as filler in a variety of applications [57]. Pitch is a by-product of coal carbonization, obtained as a residue after coal tar distillation. Pitches are known to contain of hundreds of polycyclic aro-

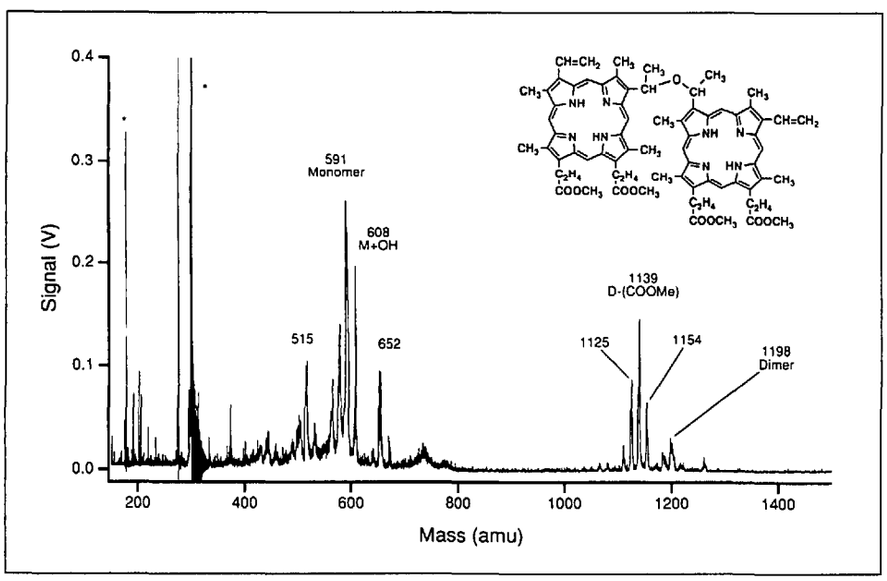

Fig. 4. *L2MS Spectrum of divinylporphyrin ether (DVE) tetramethylester (m/z = 1198).* λ(ioniz) = 243.5 nm, ionization laser power density = 1.5 x 10^5 W/cm^2. In the low mass range, signals from mass standards marked with * are visible (*m/z* 178, 267, 300). M^+ is at *m/z* 1198, fragments are found in the dimer range (1125, 1139, 1154) and in the monomer range (565, 579, 591, 608). A metastable signal at *m/z ca.* 730 is also detected.

matic hydrocarbons (PAHs), but only a small fraction of them is volatile enough to be characterized by as GC/MS GC/MS [58][59]. For example, the existence of presumably carbonaceous material with masses up to 270,000 amu has recently been shown by matrix-assisted laser desorption/ionization mass spectrometry to exist in bituminous coal [60].

Fig. 5 shows the L2MS spectrum of a pitch sample (*SGL Carbon*, Meitingen, Germany) at two different ionization wavelengths, 245 nm and 308 nm. While GC/MS can routinely analyze PAHs up to a molecular weight of *ca.* 300 amu for such materials [58][59], most of the signals obtained by L2MS actually lie above 300 amu, with signals extending to over 700 .. 800 mass units. This nicely documents the ability to access the non-volatile fraction of such materials with laser desorption. PAHs are fairly stable compounds, and no fragmentation was obtained over a wide range of laser power densities used in these investigations. The mass distribution is dependent on the ionization wavelength: the longer wavelength used (308 nm) is resonantly absorbed by larger PAHs, and is off-resonance for smaller structures, which can be seen from the absence of signals at 178 (phenanthrene/anthracene) or 192 (methyl-178) at 245 nm. The response at different wavelengths also aids in the assignment of the signals found to various possible PAH structures. For example, the signal at 302 amu is interpreted as dibenzo[*a*,*h*]pyrene, which exhibits a very large UV absorption at 310 nm, $\varepsilon \approx 1.9 \cdot 10^5$ l/(mol · cm). Other possible assignments for 302 (other benzopyrenes, dibenzofluoranthenes) have UV absorptions that are smaller by about an order of magnitude [61][62]. Further assignments are given in the caption for *Fig. 5*.

All of the signals found in this spectrum can be interpreted with a general scheme for building up more complex PAHs starting from simpler structures. This principle is illustrated in the *Scheme*. Starting from a given PAH skeleton, higher molecular weight compounds can be constructed by alkylation (*M*+14 for methylation, *M*+28 for double methylation or ethylation, *etc.*), by adding ethylene bridges (*M*+24), ethyl bridges (*M*+26), or benzo groups (*M*+50). All these homologies are found in the pitch sample investigated in *Fig. 5*. They may in fact represent the pathways of increasing carbonization of such fossilized carbonaceous material, leading ultimately to pure carbon (graphite).

Although no separation method precedes mass analysis in this case, the instrument itself behaves like a large separation device: the separation of ions according to their time of flight through the drift tube very much resembles a chromatography column! The 'chromatogram' or TOF spectrum consists of peaks that are 'eluted' in the order of their mass, a quantity much more easily interpreted than a retention time. Isomers are not separated, but techniques have been developed for carrying out tandem-TOF experiments [63–66] that allow not only structural characterization of a mass-selected parent ion by a variety of fragmentation methods, but in some cases even isomer differentiation. This analogy with chromatography can even be taken a step further. Resolution in chromatography is given by the number of theoretical plates *N*, and can be determined from the data using

$$N = 8 \ln 2 \cdot \left(\frac{t_R}{FWHM} \right)^2 \qquad (4)$$

Here, t_R is the retention time, and *FWHM* the full width at half maximum. If the quantity in parentheses is set equal to the resolution in a TOF mass spectrum, which can easily reach 1000 or more, this gives already several millions of theoretical plates, a value that is considered to be very good for chromatographic separations in a column.

Another example of the application of L2MS to complicated mixtures is shown in *Fig. 6*. This example is taken from environmental chemistry. The sample is a quartz fiber filter through which were pumped *ca.* 1/3 m^3 polluted air from a tunnel near Martigny (Switzerland). The tunnel air is fairly heavily loaded with aerosol particles, which leads to a significant darkening of a 12-mm-diam area on the filter. This darkening is monitored by the sampling instrument, an aethalometer, and can serve to estimate the amount of 'black carbon' deposited on the filter per unit time. We were interested in the chemical composition of adsorbates found on the surface of the collected aerosol particles. Although quite detailed chemical information can be obtained by extracting such samples with suitable solvents, followed by GC/MS analysis [67][68], this

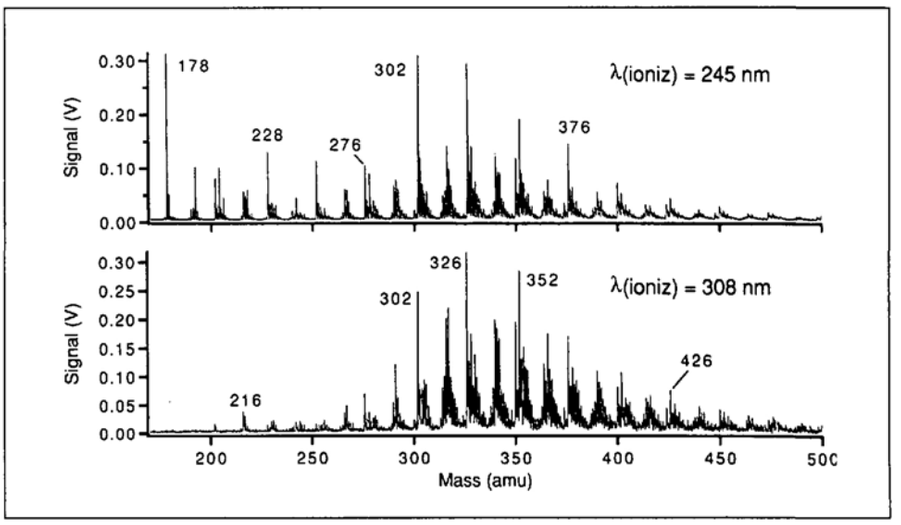

Fig. 5. *L2MS Spectrum from a petroleum pitch sample with a high m.p. and little soluble aromatic carbon contents.* Ionization wavelengths used are 245 nm (upper panel) and 308 nm (lower panel). Possible assignments of mass peaks based on polycyclic aromatic hydrocarbons are 178, phenanthrene/anthracene; 202, pyrene (fluoranthene), 216, methyl-202; 228, chrysene (triphenylene); 276, anthanthrene/benzo[*ghi*]perylene, 302, dibenzo[*a*,*h*]pyrene; 326, benzoanthanthrene; 352, tribenzopyrene (naphthobenzopyrene); 376, pyranthrene. Signals are found up to 700 .. 800 amu (not shown).

Scheme

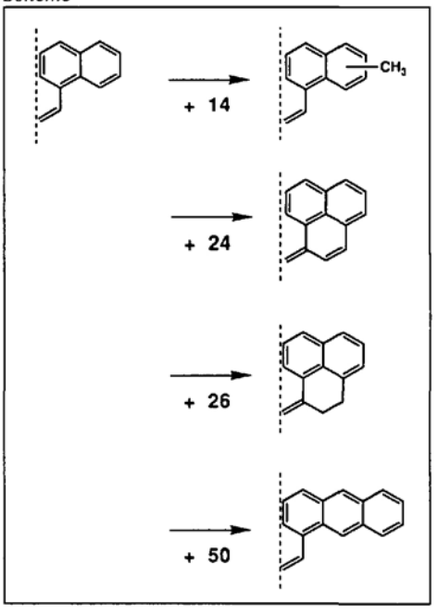

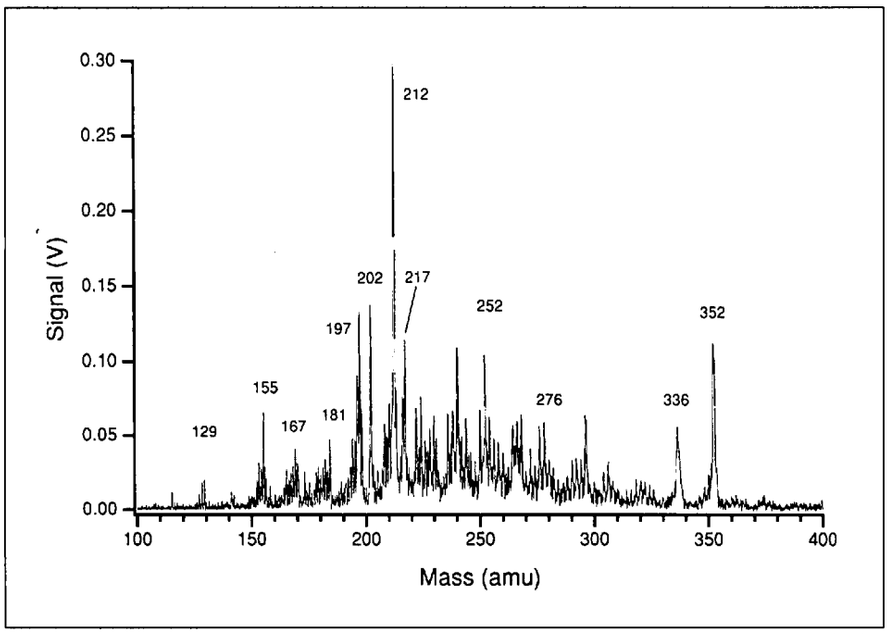

Fig. 6. *L2MS Spectrum of an aerosol sample collected in a highway tunnel near Martigny/VS.* λ(ioniz) = 308 nm. Possible peak assignments are 202, pyrene/fluoranthene; 212, nitrocarbazole/dimethyldibenzothiophene; 252, perylene; 276, anthanthrene/benzo[*ghi*]perylene; 306, tetraphenyl; 352, tribenzopyrene (naphthobenzopyrene). Many odd-mass peaks suggest the presence of nitrogen-containing aromatic compounds, *e.g.*, heteroaromatic structures, or nitro-PAHs. Possible peak identifications are: 129, quinoline; 167, carbazole; 181, methylcarbazole; 197, dimethylacridine; 217, methylazafluoranthene/benzocarbazole.

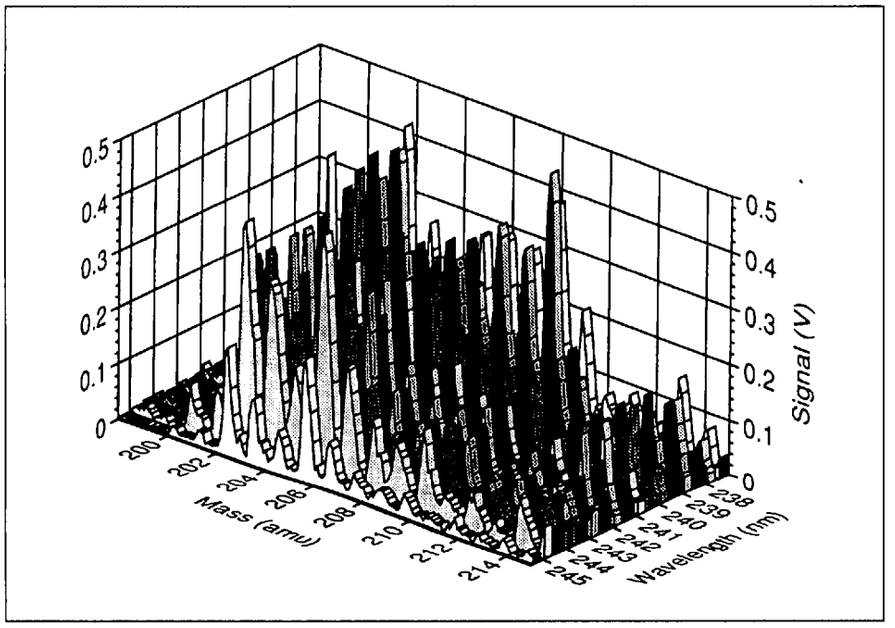

Fig. 7. *Two-dimensional UV/MS spectrum of an aerosol sample, collected in Payerne/FR.* For clarity, the mass range displayed is a small region from a much more extensive data set. Every cut perpendicular to the mass axis represents a mass-resolved UV spectrum, allowing better identification of the compounds compared to the L2MS spectrum alone.

method neither samples the non-soluble or non-volatile fraction, nor does it discriminate between the particle surfaces and their interior. However, it is the *surface properties* of the aerosol particles, *e.g.* their hydrophobicity, that determines their incorporation into the lung tissue or their expulsion once they have been inhaled. Furthermore, mutagenic properties of the chemical compounds adsorbed on particle surfaces can easily get in contact with skin or mucous membranes and thus present an obvious health hazard.

L2MS not only overcomes the limitations of GC/MS, but it also provides a much faster way of analyzing complex samples such as aerosols. In this application, the sample spot on the filter is cut to size, directly mounted on the tip of the sample holder, and introduced into the vacuum system. During this operation, which only takes a few min, the exposure of the sample to tools, chemicals, and the ambient is minimized, effectively preventing sample contamination. The L2MS data can be recorded immediately thereafter.

At first glance, the spectrum in *Fig. 6* shows some of the same peaks attributed to PAHs as those found in *Fig. 5*. However, especially in the lower mass range, there are some important differences, namely the existence of odd-mass signals. This indicates that nitrogen-containing compounds are present in the sample, for example in the form of nitro-PAHs or heteroaromatic compounds (for details see the caption of *Fig. 6*). Based on UV absorption characteristics, the base peak can be assigned to nitrocarbazole. While carbazole has its absorption maximum at *ca.* 290 nm, the NO_2 group shifts this UV absorption peak to the red by *ca.* 20 nm, into the range of the ionization wavelength used. The origin of these nitrogen-containing compounds is at present not fully understood, although the NO_x content of the tunnel air has been found to be extremely high, between 5 and 10 ppm. We surmise that nitration of PAHs can take place after their formation upon exposure to the polluted tunnel air. Alternatively, it is possible that nitrogen is already incorporated during combustion, starting with a different composition of the engine air intake.

4.3. *Two-Dimensional UV/MS Spectra*

With REMPI as an ionization method, we have an additional degree of freedom available that can be employed to extract analytical information on the sample studied. In a primitive version, this has already been shown in *Fig. 5*, where two different ionization laser wavelengths were used. *Fig. 7* shows data where the wavelength was scanned over the whole range permitted by the laser dye used in this example (coumarin 102). This experiment was carried out with another aerosol sample collected in Payerne, Switzerland. The mass spectrum is plotted in 0.5-nm intervals, and for clarity, only a small mass range from much more extensive data set is shown. This data can be used for better identification of compounds present in sample mixtures. Every cut perpendicular to the mass axis represents a mass-resolved UV spectrum, which can greatly assist in the assignment of the mass spectral peak alone. For example, the spectral trace for *m/z* 202 closely follows the UV absorption spectrum of a pyrene solution.

The 202 peak in the mass spectrum can, therefore, be assigned to pyrene with a high degree of confidence.

5. Conclusions and Outlook

Significant progress has been made towards developing L2MS into an important analytical tool. This progress is due to the high sensitivity inherent in this method, the spatial resolution in the desorption step, and the features of resonance-enhanced multiphoton ionization, *i.e.*, optically selective soft or hard ionization. If operated in the soft ionization mode, the direct chemical analysis of complex mixtures is possible using L2MS. If a range of wavelengths is used for ionization, peak identification in dense mass spectra is greatly facilitated.

Progress is also being made in our understanding of the mechanism of laser-induced thermal desorption. This will ultimately lead to adapting the desorption conditions to the requirements of the particular sample under study, and to the application of laser desorption to much more complex environments. For example, the direct analysis of tissue samples or of polymer surfaces are important analytical challenges. Using a tightly focused laser beam for desorption, the study of individual particles or even individual cells may become feasible.

Significant contributions by *Q. Zhan* and *P. Voumard* are gratefully acknowledged. This work is financially supported by the *Schweizerischer Nationalfonds zur Förderung der wissenschaftlichen Forschung* and by the *Stiftung für Stipendien auf dem Gebiete der Chemie* through the *Alfred Werner* Fellowship program.

Received: January 31, 1994

[1] R. Srinivasan, *Science* **1986**, *234*, 559.
[2] Eds. D.J. Ehrlich, G.S. Higashi, M.M. Oprrysko, *Mat. Res. Soc.* **1988**, Vol. 101.
[3] R. Srinivasan, B. Baren, *Chem. Rev.* **1989**, *89*, 1303.
[4] I.P. Herman, *Chem. Rev.* **1989**, *89*, 1323.
[5] Y.R. Shen, 'The principles of nonlinear optics', Wiley, New York, 1984.
[6] 'Surface enhanced Raman scattering', Eds. R.K. Chang and T.E. Furtak, Plenum Press, New York, 1982.
[7] H. Zacharias, *Int. J. Mod. Phys. B* **1990**, *4*, 45.
[8] R.R. Cavanagh, D.S. King, J.C. Stephenson, T.F. Heinz, *J. Phys. Chem.* **1993**, *97*, 786.
[9] J. Grotemeyer, E.W. Schlag, *Angew. Chem.* **1988**, *27*, 447.
[10] R. Zenobi, R.N. Zare, in 'Advances in Multiphoton Spectroscopy and Processes', Ed. S.H. Lin, World Scientific, Singapore, 1991, Vol. 7, p. 1.
[11] L. van Vaeck, W. van Roy, R. Gijbels, *Analusis* **1993**, *21*, 53.
[12] D.P. Land, C.L. Pettiette-Hall, R.T. McIver, J.C. Hemminger, *J. Am. Chem. Soc.* **1989**, *111*, 5970.
[13] C.L. Pettiette-Hall, D.P. Land, R.T. McIver, J.C. Hemminger, *J. Phys. Chem.* **1990**, *94*, 1948.
[14] D.P. Land, C.L. Pettiette-Hall, J.C. Hemminger, R.T. McIver, *Acc. Chem. Res.* **1991**, *24*, 42.
[15] M.A. Posthumus, P.G. Kistemaker, H.L.C. Meuzelaar, M.C. Ten Noever de Brauw, *Anal. Chem.* **1978**, *50*, 985.
[16] M. Karas, U. Bahr, A. Ingendoh, F. Hillenkamp, *Angew. Chem.* **1989**, *101*, 805.
[17] A. Vertes, R. Gijbels, in 'Laser Ionization Mass Analysis', Eds. A. Vertes, R. Gijbels, and F. Adams, John Wiley & Sons, New York, 1993, Vol. 124, p. 127.
[18] J.-J. Zhang, D.S. Nagra, L. Li, *Anal. Chem.* **1993**, *65*, 2812.
[19] K. Tanaka, H. Waki, Y. Ido, S. Akita, Y. Yoshida, T. Yoshida, *Rap. Comm. Mass Spectr.* **1988**, *2*, 151.
[20] P.O. Danis, D.E. Karr, F. Mayer, A. Holle, C. H. Watson, *Org. Mass Spectrom.* **1992**, *27*, 843.
[21] F. Hillenkamp, M. Karas, R.C. Beavis, B. T. Chait, *Anal. Chem.* **1991**, *63*, 1193A.
[22] N. Winograd, J.P. Baxter, F.M. Kimock, *Chem. Phys. Lett.* **1982**, *88*, 581.
[23] D.L. Pappas, D.M. Hrubowchak, M.H. Ervin, N. Winograd, *Science* **1989**, *243*, 64.
[24] C.H. Becker, K.T. Gillen, *Anal. Chem.* **1984**, *56*, 1671–1677.
[25] V.S. Antonov, S.E. Egorov, V.S. Letokhov, A.N. Shibanov, *JEPT Lett.* **1983**, *38*, 217.
[26] H. von Weyssenhoff, H.L. Selzle, E.W. Schlag, *Z. Naturforsch., A* **1985**, *40*, 674.
[27] R. Tembreull, D.M. Lubman, *Anal. Chem.* **1986**, *58*, 1299.
[28] R.N. Zare, J.H. Hahn, R. Zenobi, *Bull. Chem. Soc. Jpn.* **1988**, *61*, 87.
[29] D.M. Lubman, *Mass Spectrom. Rev.* **1988**, *7*, 535.
[30] U. Boesl, J. Grotemeyer, K. Walter, E.W. Schlag, *Anal. Instrum.* **1987**, *16*, 151.
[31] M.J. Dale, A. C. Jones, P.R.R. Langridge-Smith, K.F. Costello, P. G. Cummins, *Anal. Chem.* **1993**, *65*, 793.
[32] L.J. Kovalenko, C.R. Maechling, S.J. Clemett, J.-M. Philippoz, R.N. Zare, C.M. O'D. Alexander, *Anal. Chem.* **1992**, *64*, 682.
[33] M.S. de Vries, D.J. Elloway, R.Wendt, H.E. Hunziker, *Rev. Sci. Instrum.* **1992**, *63*, 3321.
[34] P. Voumard, Q. Zhan, R. Zenobi, *Rev. Sci. Instr.* **1993**, *25*, 3393.
[35] P.M. Johnson, C.E. Otis, *Ann. Rev. Phys. Chem.* **1981**, *32*, 139.
[36] W.C. Wiley, I.H. MacLaren, *Rev. Sci. Instr.* **1955**, *26*, 1150.
[37] M.V. Klein, T.E. Fourtak, 'Optics', Wiley, New York, 1986.
[38] B.A. Mamyrin, V.I. Karatev, D.V. Shmikk, V.A. Zauglin, *Sov. Phys.-JEPT* **1973**, *37*, 45.
[39] J.C.D. Brand, D.R. Williams, T.J. Cook, *J. Mol. Spectrom.* **1966**, *20*, 359.
[40] D.A. Chernoff, S.A. Rice, *J. Chem. Phys.* **1979**, *70*, 2511.
[41] J.H. Brophy, C.T. Rettner, *Chem. Phys. Lett.* **1979**, *67*, 351.
[42] V.A. Elokhin, A.N. Krutchinsky, S.E. Ryabov, *Chem. Phys. Lett.* **1990**, *170*, 193.
[43] H. Knözinger, in 'The Hydrogen Bond', Eds. P. Schuster, G. Zundel, and C. Sandorfy, North Holland Publishing Co., Amsterdam, 1976.
[44] P. Voumard, R. Zenobi, Q. Zhan, *Surf. Sci.* **1994**, in press.
[45] R.C. Beavis, B.T. Chait, *Chem. Phys. Lett.* **1991**, *181*, 479.
[46] R.N. Zare, R.D. Levine, *Chem. Phys. Lett.* **1987**, *136*, 593.
[47] R.B. Hall, S.J. Bares, in 'Chemistry and Structure at Interfaces', Eds. R.B. Hall and A.B. Ellis, VCH, Florida, 1986, p. 85.
[48] P.A. Redhead, *Vacuum* **1962**, *12*, 203.
[49] R. Zenobi, J.H. Hahn, R.N. Zare, *Chem. Phys. Lett.* **1988**, *125*, 1.
[50] J.-M. Philippoz, R. Zenobi, R.N. Zare, *Chem. Phys. Lett.* **1989**, *158*, 225.
[51] Q. Zhan, R. Zenobi, P. Voumard, to be published.
[52] T.J. Dougherty, W.R. Potter, K.R. Weishaupt, in *Prog. Clin. Biol. Res.*, Alan R. Liss, 1984, p. 301.
[53] D. Kessel, M.-L. Cheng, *Cancer Res.* **1985**, *45*, 3053.
[54] R.K. Pandey, T.J. Dougherty, K.M. Smith, *Tetrahedron Lett.* **1988**, *29*, 4657.
[55] C.J. Byrne, A.D. Ward, *Aust. J. Chem.* **1991**, *44*, 411.
[56] 'Photodynamic Therapy', Eds. B.W. Henderson and T.J. Dougherty, Marcel Dekker, New York, 1992.
[57] R. Meyer zu Reckendorf, personal communication; we thank *SGL Carbon* (Meitingen, Germany) for providing several pitch samples.
[58] C.G. Blanco, J. Blanco, P. Bernad, M.D. Guillén, *J. Chromatogr.* **1991**, *539*, 157.
[59] G. Grimmer, J. Jacob, G. Dettbarn, K.-W. Naujack, *Fres. J. Anal. Chem.* **1985**, *322*, 595.
[60] P. John, C.A.F. Johnson, J.E. Parker, G.P. Smith, A.A. Herod, C.-Z. Li, R. Kandiyoti, *Rap. Comm. Mass Spectrom.* **1993**, *7*, 795.
[61] 'Spectral atlas of polycyclic aromatic compounds', Ed. W. Karcher, Reidel, Dordrecht, 1985, Vol. 1.
[62] 'Spectral atlas of polycyclic aromatic compounds', Eds. W. Karcher and S. Ellison, Kluwer, 1988, Vol. 2.
[63] K. Schey, R.G. Cooks, A. Kraft, R. Grix, H. Wollnik, *Int. J. Mass Spectrom. Ion Proc.* **1989**, *94*, 1.
[64] R.D. Beck, P.St. John, M.M. Alvarez, F. Diederich, R.L. Whetten, *J. Phys. Chem.* **1991**, *95*, 8402.
[65] D.S. Cornett, M. Peschke, K. LaiHing, P.Y. Chemg, K.F. Willey, M.A. Duncan, *Rev. Sci. Instr.* **1992**, *63*, 2177.
[66] E.R. Williams, L. Fang, R.N. Zare, *Int. J. Mass Spectrom. Ion Processes* **1993**, *123*, 233.
[67] W.H. McClennen, N.S. Arnold, K.A. Roberts, H.L.C. Meuzelaar, J.S. Lighty, E.R. Lindgren, *Combust. Sci. Technol.* **1990**, *74*, 297.
[68] S.Y. N. Yang, D.W. Connell, D.W. Hawker, S.I. Kayal, *Sci. Tot. Environm.* **1991**, *102*, 229.